ARCHIVES OF TRANSPORT *ISSN (print):* *0866-9546*
Volume 57, Issue 1, 2021 ***e-ISSN (online):*** *2300-8830*
DOI: *10.5604/01.3001.0014.7480*

ROBUST TRAJECTORY TRACKING CONTROL FOR AUTONOMOUS VEHICLE SUBJECT TO VELOCITY-VARYING AND UNCERTAIN LATERAL DISTURBANCE

Yuqiong WANG[1], Song GAO[2], Yuhai WANG[3 4], Pengwei WANG[5], Yingchao ZHOU[6], Yi XU[7]

[1, 2, 5, 6, 7] School of Transportation and Vehicle Engineering, Shandong University of Technology, China

[3] State Key Laboratory of Automotive Simulation and Control, Jilin University, China

[4] Qingdao Automotive Research Institute, Jilin University, China

Abstract:

Autonomous vehicles are the most advanced intelligent vehicles and will play an important role in reducing traffic accidents, saving energy and reducing emission. Motion control for trajectory tracking is one of the core issues in the field of autonomous vehicle research. According to the characteristics of strong nonlinearity, uncertainty and changing longitudinal velocity for autonomous vehicles at high speed steering condition, the robust trajectory tracking control is studied. Firstly, the vehicle system models are established and the novel target longitudinal velocity planning is carried out. This velocity planning method can not only ensure that the autonomous vehicle operates in a strong nonlinear coupling state in bend, but also easy to be constructed. Then, taking the lateral location deviation minimizing to zero as the lateral control objective, a robust active disturbance rejection control path tracking controller is designed along with an extended state observer which can deal with the varying velocity and uncertain lateral disturbance effectively. Additionally, the feedforward-feedback control method is adopted to control the total tire torque, which is distributed according to the steering characteristics of the vehicle for additional yaw moment to enhance vehicle handing stability. Finally, the robustness of the proposed controller is evaluated under velocity-varying condition and sudden lateral disturbance. The single-lane change maneuver and double-lane change maneuver under vary longitudinal velocity and different road adhesions are both simulated. The simulation results based on Matlab/Simulink show that the proposed controller can accurately observe the external disturbances and have good performance in trajectory tracking and handing stability. The maximum lateral error reduces by 0.18 meters compared with a vehicle that controlled by a feedback-feedforward path tracking controller in the single-lane change maneuver. The lateral deviation is still very small even in the double lane change case of abrupt curvature. It should be noted that our proposed control algorithm is simple and robust, thus provide great potential for engineering application.

Keywords: *autonomous vehicle, path tracking, velocity tracking, active disturbance rejection control, robustness*

To cite this article:

Wang, Y., Gao, S., Wang, Y., Wang, P., Zhou, Y., Xu, Y., 2021. Robust trajectory tracking control for autonomous vehicle subject to velocity-varying and uncertain lateral disturbance. Archives of Transport, 57(1), 7-23. DOI: https://doi.org/10.5604/01.3001.0014.7480

Contact:
1) wangyuqiong@sudt.edu.cn [https://orcid.org/0000-0001-8624-7298], 2) gaosongsdut@163.com [https://orcid.org/0000-0002-3367-2546] - corresponding author, 3) yuhaiwang77@163.com [https://orcid.org/0000-0001-8810-2076], 4) wpwk16@163.com [https://orcid.org/0000-0001-6827-0988], 5) zhouyc_sdut@163.com [https://orcid.org/0000-0002-3700-2267], 6) xuyisdut@163.com [https://orcid.org/0000-0001-8624-7298] – corresponding author

1. Introduction

Intelligent vehicle technology has attracted increasingly attention with the rapid development of internet communication technology, computer artificial intelligence and other technologies (Wang et al., 2001). Autonomous vehicles are the most advanced of intelligent vehicles and will play an important role in reducing traffic accidents, saving energy and reducing emission (Hu et al., 2016; Wang et al., 2020). Motion control for trajectory tracking is one of the core issues in the field of autonomous vehicle research besides the environment perception, dynamic decision and planning. The most important thing is to obtain effective throttle, braking and steering action within the vehicle through trajectory tracking control (Amer et al., 2017).

The vehicle models should be established before the trajectory tracking control. Many vehicle models had been utilized in autonomous vehicle path tracking control. Van N. D. et al. studied the steering control of autonomous vehicles based on the pure pursuit model which was the most commonly used geometric model (Van et al., 2020). However, the geometric model was based on the Ackerman steering principle and could only be used in low-speed linear condition. The kinematic model was utilized for the trajectory planning and tracking in (Zhang et al., 2019), but the dynamic characteristics of the vehicle were not taken into account. The dynamic model (Zhao et al., 2011; Cai et al., 2018; Gao et al., 2018; Chen et al., 2019) had been widely used because it can be applied to the high-speed nonlinear condition, especially to the limit conditions.

Based on the vehicle dynamic model, the proportion-integral-derivative (PID) algorithm was utilized to control the yaw angle deviation approaching to zero and verified the effectiveness of the controller by real vehicle test (Zhao et al., 2011; Cai et al., 2018). However, PID controller is sensitive to the change of system parameters and the adaptability of the controller parameters to the vehicle speed is relatively weak. Hamilton energy function control could make the system achieve local or global optimization under some conditions such as automatic emergency obstacle avoidance (Gao et al., 2018,) and path tracking (Chen et al., 2019). However, the optimal control method relied on accurate mathematical model and cannot suppress the disturbance caused by the change of parameters and uncertain disturbance.

Since the autonomous vehicles often suffered by the internal parameter uncertainty and external disturbance, the robust control methods were widely used in trajectory tracking of autonomous vehicles. Model predictive control has been widely used in vehicle motion control (Sun et al., 2018; Cheng et al., 2020; Guo et al., 2020; Lin et al., 2019) owing to its good robustness, but it need to give consideration to the model accuracy, calculation complexity and real-time performance. A robust $H\infty$ state-feedback controller is proposed to achieve the path following and vehicle lateral control simultaneously (Wang et al., 2016). (Ardashir et al., 2020) proposed an adaptive control based on immersion and invariance control theorem for trajectory tracking of autonomous vehicles subject to uncertain dynamics. An adaptive neural-network-based steering controller was proposed for autonomous vehicle at handing limits which had good robustness against different road adhesion (Ji et al., 2018). Active disturbance rejection control (ADRC) also had been used in autonomous vehicle tracking control (Xia et al., 2016; Wu et al., 2019; Yan et al., 2019). The ADRC algorithm was established and developed by Jingqing Han et al (Han et al., 2002; Gao et al., 2013), and the stability analysis had been proved in (Wu et al., 2018). The ADRC can provide potentials to improve robustness by observing and compensating the modelling uncertainty and external disturbance. However, the construction of the desired yaw angle increases the difficulty of parameter adjustment, and the steady-state lateral deviation may occur when the parameters are not adjusted properly (Wu et al., 2019; Yan et al., 2019).

These control methods were all robustly, but few researches devoted to velocity-varying conditions. Nevertheless, vehicle longitudinal velocity varies when a car runs on a road, and the variable longitudinal velocity has a great impact on vehicle steering stability since the strong coupling dynamics exist between the longitudinal and lateral motion. Nam D. V. applied an adaptive pure pursuit-based steering controller besides a longitudinal controller and verified its robustness via real vehicle tests (Van et al., 2020). However, the robustness of high-speed conditions was not considered since the coupling of longitudinal and lateral motion was not strong with low longitudinal velocity and lateral acceleration. Nitin R. K. et al. designed a feedforward-feedback steer-

ing controller for both accurate path tracking and lateral stability at vehicle handling limits (Kapania et al., 2015). Nonlinear model inversion control was presented to control the position and sideslip of the autonomous vehicle approaching to the desired trajectory (Goh et al., 2019). Erik W. employed the State Dependent Riccati Equation technique to design a feedback-feedforward steering controller which showed robust path tracking performance even when the rear wheels reaches their friction limits, and large body sideslip prevails (Wachter et al., 2019). These papers (Kapania et al., 2015; Goh et al., 2019; Wachter et al., 2019) had considered the change of longitudinal velocity, and the control methods had been proved to be robust to different road curvature. However, the robustness to the unknown strong disturbances was not discussed. So the vehicle trajectory tracking control subject to both velocity-varying and uncertain disturbance at high speed is still worth to study.

In this paper, the uncertainty dynamics, external disturbances and the change of longitudinal velocity are considered simultaneously. The active disturbance rejection control (ADRC) with extended state observer (ESO) is used to control the lateral motion of the autonomous vehicle aiming at zero lateral deviation; the feedforward-feedback control method is used to control the longitudinal motion, so as to achieve the precise trajectory tracking of the autonomous vehicle under velocity-varying conditions. The main contributions of this paper are as follows:

(1) A new longitudinal velocity planning method is proposed to approach the adhesion limit at the maximum curve;
(2) The velocity tracking for autonomous vehicle is completed besides path tracking aiming at the high-speed emergency obstacle avoidance;
(3) To deal with the varying velocity and uncertain external disturbances, the extended state observer is employed in the controller design.

The rest of this paper is organized as follows. The system modelling and longitudinal velocity planning are presented in section II and section III. Section IV gives a detailed description about the trajectory tracking controller design. Section V presents the simulation verification of different control algorithm's performance and robustness. Section VI is the conclusion.

2. System Modelling

2.1. Vehicle dynamics model

In order to study the trajectory tracking performance of autonomous vehicle under the longitudinal and lateral coupling motions such as obstacle avoidance at high-speed, the planar motion stability is mainly considered than roll or pitch stability. Thus the impacts of suspension system and road inequality are ignored in this paper. So the three degrees of freedom vehicle model concluding longitudinal motion, lateral motion and yaw motion is established. Figure 1 shows the vehicle system model. In the figure, *OXY* is the absolute coordinate system, *oxy* is the vehicle coordinate system:

- l_f, l_r are the distance from the vehicle centre of mass to the front axle and rear axle respectively;
- δ_f is the front wheel angle;
- F_{yfl}, F_{yfr}, F_{yrl}, F_{yrr} are the lateral forces on the left front wheel, right front wheel, left rear wheel and right rear wheel respectively;
- F_{xfl}, F_{xfr}, F_{xrl}, F_{xrr} are respectively the longitudinal forces on the left front wheel, the right front wheel, the left rear wheel and the right rear wheel;
- v is the vehicle's centroid speed;
- v_x is the vehicle's longitudinal speed at the centroid;
- v_y is the vehicle's lateral speed at the centroid;
- β is the vehicle's centroid sideslip angle;
- w is the vehicle's yaw rate.

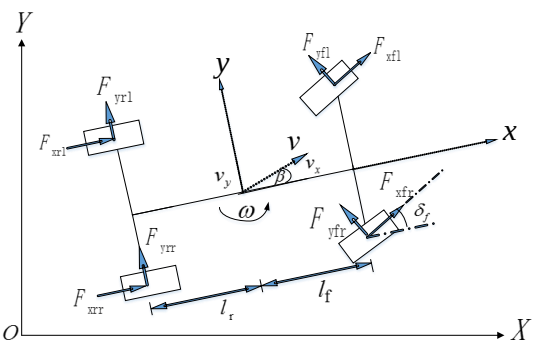

Fig. 1. Vehicle system model

$$\begin{cases} \dot{v}_x = v_y\dot{\psi} + (F_{xf}\cos\delta_f - F_{yf}\sin\delta_f + F_{xr})/m \\ \dot{v}_y = -v_x\dot{\psi} + (F_{xf}\sin\delta_f + F_{yf}\cos\delta_f + F_{yr} + F_{fw})/m \\ \dot{w} = (F_{xf}l_f\sin\delta_f + F_{yf}l_f\cos\delta_f - F_{yr}l_r + \Delta M)/I_z \\ \dot{Y} = v_x\sin\psi + v_y\cos\psi \\ \dot{X} = v_x\cos\psi - v_y\sin\psi \end{cases} \quad (1)$$

Where X and Y are the longitudinal and lateral displacement of the vehicle in OXY coordinate; ψ is the yaw angle of the vehicle ; F_{yf}, F_{yr}, F_{xf}, F_{xr} are the lateral and longitudinal tire forces of front and rear axles respectively; F_{fw} is the disturbance of uncertainty dynamic and external disturbances such as lateral wind; m is the mass of the vehicle; ΔM is the additional yaw produced by the longitudinal force of the tires; I_z is the yaw moment of inertia of vehicle.

2.2. Tire model

The main purpose of this paper is trajectory tracking control subject to velocity varying and uncertain disturbance. So the vehicle longitudinal and lateral coupled control will be studied in this paper. The nonlinear coupling of longitudinal and lateral tire forces is one of the main coupling influence factors besides the lateral-longitudinal-yaw motion coupling and vertical load transfer. The magic formula by H.B Pacejka prevails (Pacejka et al., 2006) is utilized to describe the coupling dynamics of tires.

The pure longitudinal and lateral tire forces can be calculated by the magic formula as follows:

$$\begin{aligned} F_{x0} &= D_x sin\,(C_x arctan\,(B_x s - E_x(B_x s - arctan(B_x s))) \\ F_{y0} &= D_y \sin\,(C_y \arctan\,(B_y \alpha - E_y(B_y \alpha - \arctan(B_y \alpha))) \end{aligned} \quad (2)$$

Where s represents tire slip ratio; α is the sideslip angle. C_x=1.65; C_y=1.3; and according to (2):

$$\begin{aligned} D_x &= \mu(a_1 {F_z}^2 + a_2 F_z) \\ B_x &= (a_3 {F_z}^2 + a_4 F_z)\exp(-a_5 F_z)/(C_x D_x) \\ E_x &= a_6 {F_z}^2 + a_7 F + a_8 \\ D_y &= \mu(b_1 {F_z}^2 + b_2 F_z) \\ B_y &= (b_3 {F_z}^2 + b_4 F_z)\exp(-b_5 F_z)/(C_y D_y) \\ E_y &= b_6 {F_z}^2 + b_7 F + b_8 \end{aligned}$$

Where, a_m and b_n are fitting coefficients, m and n represent the number of 1 to 8; F_z is the vertical force of the tire which can be expressed based on the roll dynamics and pitch dynamics; μ is the road adhesion coefficient.

In the combined longitudinal and lateral operation condition, the comprehensive slip ratio can be explained as equation (3)

$$\sigma = \sqrt{{\sigma_x}^2 + {\sigma_y}^2} \quad (3)$$

Where $\sigma_x = \frac{-s}{1+s}$; $\sigma_y = \frac{-\tan\alpha}{1+s}$.

Then, the combined longitudinal and lateral tire forces yield.

$$F_x = -\frac{\sigma_x}{\sigma}F_{x0}; F_y = -\frac{\sigma_y}{\sigma}F_{y0}c \quad (4)$$

Introducing the concept of equivalent lateral cornering stiffness (5), the tire model (2) can be simplified formally. The equivalent cornering stiffness is the real-time derivative of tire force to the tire sideslip angle, which is changeable at any time, and still conforms to the coupling nonlinear characteristics in (2).

$$\begin{cases} \hat{C}_f = \partial F_{yf}/\partial\alpha_f \\ \hat{C}_r = \partial F_{yr}/\partial\alpha_r \end{cases} \quad (5)$$

Where and represent the equivalent lateral cornering stiffness of front and rear axles, respectively.

The sideslip angel of front and rear wheels can be expressed as Equation (6) based on the small angle hypothesis.

$$\begin{cases} \alpha_f = -(\frac{v_y + w l_f}{v_x} - \delta_f) \\ \alpha_r = -\frac{v_y - w l_r}{v_x} \end{cases} \quad (6)$$

In order to introduce the tire torque to the controller design, the longitudinal tire fore can also be calculated as follows:

$$F_x = F_{xf} + F_{xr} = (-I_w(\dot{w}_f + \dot{w}_r) + T_w)/R_w \quad (7)$$

Where Tw is the sum of total driving torque and braking torque vector of front and rear axles; Iw represents the wheel yaw moment of inertia, Rw represents the wheel rolling radius, ωf and ωr are the angular velocity of front and rear wheels, respectively.

3. Longitudinal Velocity Planning

Currently, velocity planning had appears in lateral tracking under normal and extreme conditions (Goh et al., 2016, Guo et al., 2018, Wang et al., 2016; Kapania et al., 2016). The “quasi-equilibrium” strategy

was used for a simple path generation and the reference sideslip angel was constructed as a function of path distance by aid of equilibrium point solution (Goh et al., 2019; Goh et al., 2016,). The reference velocity was yielded by solving the 3DOF vehicle dynamic equations under equilibrium states. However, not all paths are based on this "quasi-equilibrium" strategy. For a general path, the velocity planning generally falls into two categories. One is following the rule of decelerating entry in bends and accelerating out of the bends, but the speed and acceleration in initial positions and in bends can be set arbitrarily. This velocity profile construction method is simple and can be seen in (Guo et al., 2018, Wang et al., 2019). However, the velocity in any points does not approach the adhesion limit. Another method considers approaching the limit of adhesion, lateral stability criteria and the driving/braking actuator all the time (Kapania et al., 2016). Kapania N.R. took three steps to generate the velocity profile aimed at the minimum lap time: giving zero longitudinal force to plan velocity profile, then updating velocity profile after forward pass and backward pass. However, the path construction process is complex and should be re-planned because this profile was obtained based on the ideal steady state according to the reference path.

In this paper, the combination of the above two methods is adopted for a general path. On one hand, the reference longitudinal velocity and acceleration are designed according to the principle of slowing down before the start of the curve and accelerating after the curve. On the other hand, the velocity profile approaches the adhesion limit at the maximum curve location. This velocity-planning method can not only ensure that the autonomous vehicle operates in a strong nonlinear coupling state in bend, but also easy to be constructed.

3.1. Reference acceleration generation

The reference longitudinal acceleration is generated considering the road curvature and the comfort of passengers. Thus the longitudinal acceleration changes from zero, rather than braking suddenly with a large acceleration when autonomous vehicle enters in a curve. Since the velocity entering and leaving the curve is closely related to the curvature of the road, it is considered to express the expected longitudinal acceleration as a function of the road curvature, as shown in formula (8).

$$a_x{}^r = -\lambda\rho_r \mathrm{sign}(\dot{\rho}_r) \tag{8}$$

where λ is a positive constant. The greater the constant is, the closer the vehicle reaches to the adhesion limit at the maximum bend.

3.2. Road information criteria

The longitudinal and lateral acceleration shall meet the adhesion conditions when the vehicle steers on the road.

$$\sqrt{a_x{}^2 + a_y{}^2} \le \mu g \tag{9}$$

where g=9.8 *m/s*^{2}, ay represents vehicle lateral acceleration which can be calculated by longitudinal velocity and the road curvature as equation (11) shows.

$$a_y{=}\rho v_x{}^2 \tag{10}$$

4. Controller Design

4.1. Overall control strategy

Figure 2 shows the block diagram of the control system proposed in this paper. We take the front wheel angle, driving and braking torque of the tires as input of the autonomous vehicle ignoring the influence of steering system and traveling system.

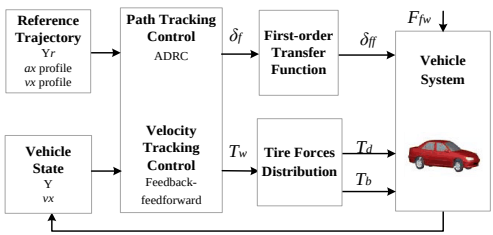

Fig. 2. The overall control frame

There are two parts of the control system and they interact with each other because of the vehicle vertical load transfer, the coupling of longitudinal and lateral tire force, and vehicle longitudinal-lateral-yaw motion coupling. Considering the time delay of the control system, a first-order delay link is introduced to simulate the front wheel angle delay of the control system, so as to avoid the instability or even vibration during the real vehicle control. In addition, additional yaw is generated to provide great potential for lateral stability through differential braking.

4.2. Lateral path tracking controller design

Substitute equation (6) and (7) into equation (1), the second derivative of Y can be calculated based on small angle hypothesis.

$$\begin{aligned}\ddot{Y} &= \dot{v}_x \sin\psi + \dot{v}_y \cos\psi + \dot{X}\dot{\psi} \\ &= \left(\frac{\hat{C}_f}{m} + \frac{T_w - I_w \dot{w}_f}{mR_w}\right)\delta_f - \frac{v_y(\hat{C}_f + \hat{C}_r) + \dot{\psi}(\hat{C}_f l_f - \hat{C}_r l_r)}{m v_x} \\ &\quad -v_x\dot{\psi} + \dot{v}_x\psi + \dot{X}\dot{\psi} + \frac{F_w}{m}\end{aligned} \tag{11}$$

Since the coefficient of front wheel angle contains input T_w and state variable $\dot{w}_f$, which are time-varying. Thus, constant b and variable b_w are introduced, and the relationship is as follows:

$$b_w + b = \frac{\hat{C}_f}{m} + \frac{T_w - I_w \dot{w}_f}{mR_w} \tag{12}$$

Take time-varying as disturbance, and Equation (11) can be rewritten as follows:

$$\begin{aligned}&Y = x_1, \dot{Y} = x_2, \ddot{Y} = \dot{x}_2, \\ &f_w = b_w\delta_f - \frac{v_y(\hat{C}_f + \hat{C}_r) + \dot{\psi}(\hat{C}_f l_f - \hat{C}_r l_r)}{m v_x} \\ &-v_x\dot{\psi} + \dot{v}_x\psi + \dot{X}\dot{\psi} + \frac{F_w}{m}\end{aligned} \tag{13}$$

Equation (4) can be expressed as the standard form of integrator series system:

$$\begin{cases} \dot{x}_1 = x_2 \\ \dot{x}_2 = b\delta_f + f_w \\ y = x_1 \end{cases} \tag{14}$$

Where f_w is the sum of uncertain dynamics and unknown disturbances of the system; y is the output of the system.

In this paper, active disturbance rejection control (ADRC) is utilized to observe and compensate the modelling uncertainty and external disturbance, and then make the autonomous vehicle track the reference path.

The whole ADRC consists of three modules: tracking differentiator (TD), nonlinear combination law (NCL) and extended state observer (ESO). TD is utilized to extract a smooth input signal and its differential signal; ESO provides potentials for the observing and compensating of the un-modeled dynamic and unknown disturbance; NCL takes the output error between ESO and TD to determine the control output. The control frame of the ADRC is shown in Figure 3.

The tracking differentiator utilizes the "fast control optimal synthesis function" to track the reference differential signal rapidly, which avoids extracting derivatives from the tracking error. The total disturbance is taken as the expanded state variable in the design of extended state observer, and the uncertain system is dynamically linearized in real time. Then, the un-modelled dynamic and unknown disturbance can be observed and compensated. The nonlinear combination part uses output error between TD and ESO to determine the control output δ_{f0} and uses the estimated value of the disturbance to compensate system in order to obtain the final control output δ_f.

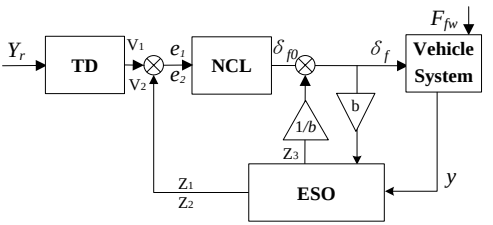

Fig. 3. Lateral path tracking ADRC controller

4.2.1. TD

The discrete form of system (14) is:

$$\begin{cases} x_1(k+1) = x_1(k) + hx_2(k) \\ x_2(k+1) = x_2(k) + hu, |u| \le r \end{cases} \tag{15}$$

The fast control optimal synthesis function obtained from the above formula is as follows:

$$\begin{cases} d = rh; d_0 = dh \\ c = x_1 + hx_2 \\ a_0 = (^{a^2} + 8r|c|^{1/2}) \\ a = \begin{cases} x_2 + (a_0 - d)/2 & |c| > d_0 \\ x_2 + c/h & |c| \le d_0 \end{cases} \\ u = -\begin{cases} ra/d & |a| \le d \\ r\mathrm{sgn}(a) & |a| > d \end{cases} \end{cases} \tag{16}$$

Where, h is the simulation integration step, and $0.001s$ is taken in this paper; the controller design parameter r represents the speed factor, which determines the tracking speed and is generally selected with a larger value.

4.2.2. ESO

Set $x_3 = f_w, \dot{x}_3 = g_w$.

Take f_w as a new state variable x_3 assuming that f_w is bounded and can be differentiated into g_w, then the equation (6) can be expanded into the control system as follows:

$$\begin{cases} \dot{x}_1 = x_2 \\ \dot{x}_2 = b\delta_f + f_w \\ y = x_1 \end{cases} \tag{17}$$

Set the output of the state observer as z_1、z_2 and z_3, which are the observation values of y、$\dot{y}$and f_w respectively. Then, the observation error of the system output is:

$$e = z_1 - y \tag{18}$$

The state equation of the observer is shown in equation (19).

$$\begin{cases} \dot{z}_1 = z_2 - \beta_1 e \\ \dot{z}_2 = b\delta_f + z_3 - \beta_2 fal_1(e, \alpha_1, \delta) \\ \dot{z}_3 = -\beta_3 fal_2(e, \alpha_2, \delta) \end{cases} \tag{19}$$

where:

$$\beta_1 = 3w_0, \beta_2 = 3w_0^2, \beta_3 = 3w_0^3 \tag{20}$$

$$\begin{cases} fal_1 = \begin{cases} |e| sign(e) & |e| \geq \delta \\ \frac{e}{\delta^{(1-\alpha_1)}} & |e| < \delta \end{cases} \\ fal_2 = \begin{cases} |e| sign(e) & |e| \geq \delta \\ \frac{e}{\delta^{(1-\alpha_2)}} & |e| < \delta \end{cases} \end{cases} \tag{21}$$

Where, w_0 can be seen as the wideband of the observer which affects the observer tracking speed significantly. The accuracy of the estimation is positively related to the value of w_0. However, the noise sensitivity may increase if the observer bandwidth is too large. An appropriate value of w_0 can estimate total disturbance z_3 accurately tracking f_w. The observer can converge when the observer wideband is expressed as formula (11) (Wu et al., 2018). $\alpha_1, \alpha_2, \delta$ is the controller design parameters, the general selection range is $\alpha_2 < \alpha_1$, which can be taken as $\alpha_1 = 0.5, \alpha_1 = 0.25$ (Han et al., 2002).

4.2.3. NCL

Assuming the output and its differential signal after the TD are v_1 and v_2 respectively, the deviation between the TD output and the ESO output will be:

$$\begin{cases} e_1 = v_1 - z_1 \\ e_2 = v_2 - z_2 \end{cases} \tag{22}$$

The nonlinear PD control law is designed by using the characteristic of *fal* function as equation (14).

$$\delta_{f0} = k_p fal_3(e_1, \alpha_3, \delta) + k_d fal_4(e_2, \alpha_4, \delta) \tag{23}$$

In the formula (23), the *fal* function is the similar as (21), in which the general selection range of α_3, α_4 is $0 < \alpha_3 \leq 1 \leq \alpha_4$ (Han et al., 2002); *kp* and *kd* are the design parameters, which are selected by experience.

Then, the lateral controller input can be expressed as equation (24) which can similarly linearize the system as system (25). This is the real-time dynamic linearization of uncertain systems.

$$\delta_f = \delta_{f0} - z_3/b \tag{24}$$

$$\begin{cases} \dot{x}_1 = x_2 \\ \dot{x}_2 = b\delta_{f0} \\ y = x_1 \end{cases} \tag{25}$$

4.3. Longitudinal velocity tracking controller

The longitudinal velocity controller is carried out in the way of feedforward and feedback control, as shown in Figure 4.

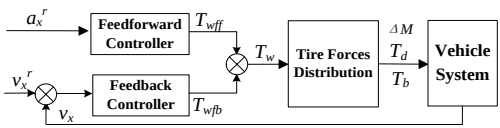

Fig. 4. Longitudinal velocity tracking feedback-feedforward controller

4.3.1. Feedforward controller

Based on Newton's second law, the feedforward longitudinal torque of tires can be calculated since the reference longitudinal acceleration is known. Substitute equation (6) and the references into equation (1):

$$\dot{v}_x^{ref} = v_y\dot{\psi} + ((-I_w(\dot{w}_f + \dot{w}_r) + T_{wff}) / R_w - F_{yf}\sin\delta_f) / m \tag{26}$$

Where, T_{wff} represents the feedforward tire torque and can be explained as the following equation (27).

$$T_{wff} = \left(m\dot{v}_x{}^{ref} - mv_y\dot{\psi} + F_{yf}\sin\delta_f\right)R_w + I_w(\dot{w}_f + \dot{w}_r) \quad (27)$$

4.3.2. Feedback controller

Since the longitudinal velocity profile is designed in Section 2, a feedback controller is designed based on the error between the reference and actual longitudinal velocity.

If the desired longitudinal speed of intelligent vehicle is $v_x{}^r$ and proportional feedback control is adopted, the feedback tire torque T_{wfb} is:

$$T_{wfb} = k(v_x^r - v_x) \quad (28)$$

Where, T_{wfb} represents the feedback tire torque; $v_x{}^r$ is desired longitudinal velocity; k represents the proportional factor.

Adding the feedforward tire torque (27) and feedback tire torque (28) yields the total tire torque T_w.

$$T_w = T_{wff} + T_{wfd} \quad (29)$$

4.3.3. Tire torque distribution

Ignoring the modelling of engine and transmission systems, it is assumed that the driving torque and braking torque are directly applied to the tires. Thus Tw is treated as driving torque when T_w>0, and as braking torque contrarily when T_w<0. Assuming rear tires are the driving tires when in drive mode.

The additional yaw moment can provide potentials to improve lateral stability of the autonomous vehicle (Wu et al., 2017; Cheng et al., 2020). Therefore, the tire torque distribution is adopted to generate additional yaw moment for vehicle stability, while meeting the longitudinal force demand to ensure the speed tracking.

The additional yaw moment yielded by the braking torques can be calculated as following:

$$\Delta M = \frac{\sum(-1)^{i+1}T_{bi}S_{bi}}{R_w} \quad i = 1,2,3,4 \quad (30)$$

Where, the S_{bi} denotes horizontal distance between the four wheels and the vehicle centroid, T_{bi} represents the braking torque of the four wheel, and i denotes the front axle left wheel, front axle right wheel, rear axle left wheel, rear axle right wheel respectively. The braking torque is distributed according to the steering characteristics of the vehicle which can be characterized by stability factor K.

$$K = \frac{m}{(l_f+l_r)^2}\left(\frac{l_f}{C_r} - \frac{l_r}{C_f}\right) \quad (31)$$

The vehicle is over-steer when K is less than zero, and the vehicle is under-steer when K is above zero. The single wheel braking strategy can be explained as table 1 (Yu et al., 2007).

Table 1. The tire torques distribution strategy

Tire torques distribution strategy	Working condition
$T_{drl}=T_{drr}=0.5T_w$, $T_{dfl}=T_{dfr}=0$	T_w >0
$T_{b2}=-T_w$, $T_{b1}=T_{b3}=T_{b4}=0$	T_w <0, turn left, K<0
$T_{b1}=-T_w$, $T_{b2}=T_{b3}=T_{b4}=0$	T_w <0, turn right, K<0
$T_{b3}=-T_w$, $T_{b1}=T_{b2}=T_{b4}=0$	T_w <0, turn left, K>0
$T_{b4}=-T_w$, $T_{b1}=T_{b2}=T_{b3}=0$	T_w <0, turn right, K>0

5. Simulation Results

In order to verify the -robustness of our proposed trajectory tracking controller subject to velocity-varying and external disturbance, a 10 DOF vehicle body and tire system model is established by Matlab/Simulink, and the simulation verification of different working conditions is carried out. The main parameters of the autonomous vehicle are shown in Table 2. The controller parameters are as follows: r = 10000; α_3 = 0.75; α_4 = 1.5; w_0 = 10; b = 83; k_p = 0.01; k_d = 12; k = 40

The results of the proposed robust ADRC algorithm are compared with the feedback-feedforward steering controllers in (Kapania et al., 2015). The traditional heading deviation Δφ and amended heading deviation Δφ+β are set as control targets separately, we name the feedback-feedforward steering controllers as "FB-FF controller with Δφ" and "FB-FF controller with Δφ+β" accordingly. The constant cornering stiffnesses and real sideslip angle are used for calculation of the surveyed controllers. The design parameters of the surveyed controllers are as follows: K_P = 0.6, x_I = 20.

Table 2. Main vehicle parameters

Parameters	Symbol	Value	Units
Vehicle mass	m	1515	kg
Yaw inertia	I_z	1680	$kg.m^2$
Distance between front axle to vehicle centroid	l_f	1.209	m
Distance between rear axle to vehicle centroid	lr	1.553	m
Nominal front axle cornering stiffness	C_f	-118000	N/rad
Nominal rear axle cornering stiffness	C_r	-108000	N/rad

5.1. Single-Lane Change Maneuver

In the simulation, a single-lane change maneuver similar with that in (Wang et al., 2016) is completed for the vehicle at the initial speed of 30 m/s on the low-adherence road ($\mu = 0.2$) while suffering from a strong lateral disturbance at t = 3.5s to t = 4.5s as Figure 5 shows. The lateral disturbance such as strong wind plays a significant role in road safety which may be affected the moving vehicle thus resulting sideslip (Betkier et al., 2019). The max lateral wind is set as 1000N which is twice that mentioned in reference (Shirazi et al., 2018). Figure 6(a) shows the road curvature varying with the vehicle travel distance. The reference longitudinal acceleration is plotted in Figure 6(b) from which one can see that the absolute value of longitudinal acceleration at the maximum curvature is the largest.

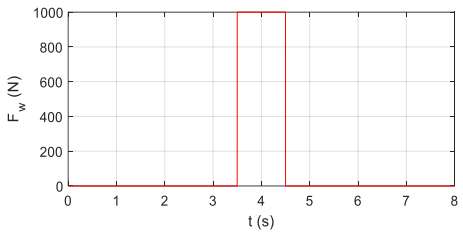

Fig. 5. Sudden lateral disturbance

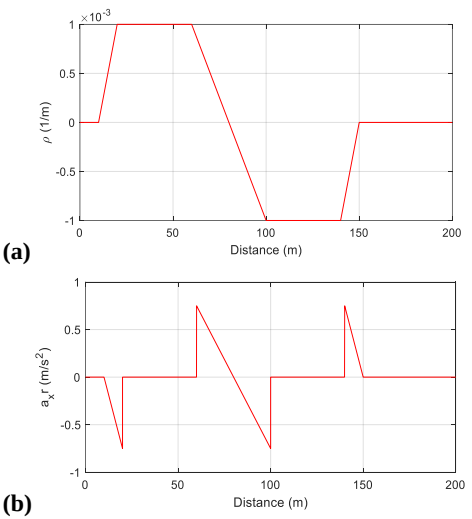

Fig. 6. Reference road curvature and longitudinal acceleration in single-lane maneuver: **(a)** Reference road curvature; **(b)** Reference longitudinal acceleration

Figure 7.A. and 7.B. shows the trajectory tracking results with the proposed controller and surveyed controllers. Figure 7.A. (a)-(b) and 7.B. (c)-(d) present vehicle global displacement, lateral offset, traditional vehicle heading error, and amended velocity heading error respectively. It can be seen that the lateral offset of FB-FF controller based on vehicle heading deviation $\Delta\varphi$ is much larger than the other controllers. The FB-FF controller based on amended velocity heading deviation $\Delta\varphi+\beta$ provides great potential for reducing lateral displacement deviation and velocity heading deviation. However, the proposed controller performs best on path tracking errors. The max absolute deviation and integral time-weighted absolute error (Zhao et al., 2011) of the lateral displacement and vehicle heading deviation with different controllers are shown in Table 3.

Table 3. Tracking error comparison of different controllers

Controller	Max(e_y)	ITAE(e_y)
FB-FF controller with $\Delta\varphi$	0.1860	1.701
FB-FF controller with $\Delta\varphi+\beta$	0.0086	0.179
Proposed controller	0.0023	0.034

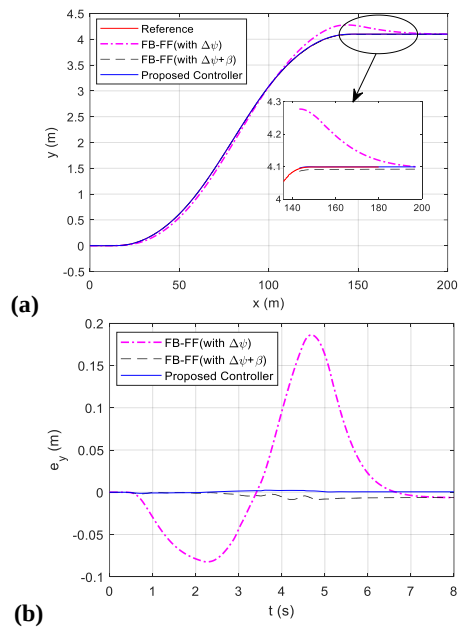

Fig. 7.A. The path following trajectory and tracking errors results in single-lane maneuver. **(a)** Path following trajectory results; **(b)** Lateral offset results

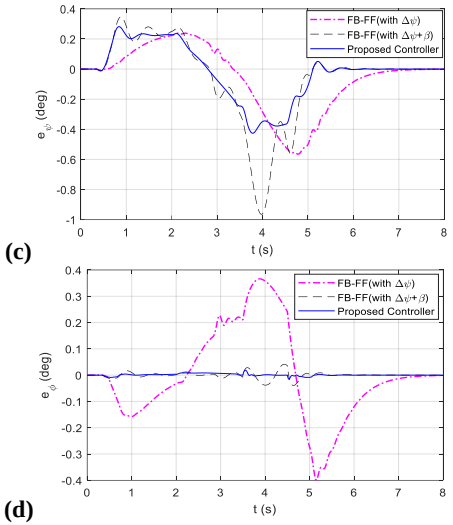

Fig. 7.B. The path following trajectory and tracking errors results in single-lane maneuver. **(c)** Vehicle heading error results; **(d)** Velocity heading error results

The sideslip angle, lateral velocity and acceleration are shown in the Figure 8, we can see that the proposed controller can yield minimum responses and maintain them in the more stability regions. The lateral acceleration of the proposed controller responds fast when suffering a sudden lateral disturbance at t = 3.5s and t = 4.5s, and the sideslip angle, yaw rate, lateral velocity increase when the external disturbance is introduced. The FB-FF controller with Δφ is dedicated to eliminating yaw angle deviation, thus yield smooth yaw rate response as sub-figure (d) shows.

The longitudinal velocity and the corresponding control input total tire torque are plotted in Figure 9, from which we can see that changing trends of the tire torque are much similar as that of reference longitudinal acceleration, and the longitudinal velocity can vary roughly with the expected value. Figure 10 shows the simulation results of the front-wheel steering angle. It can be seen that the front-wheel steering angle controlled by the proposed controller changes with the road curvature roughly. The front-wheel steering angle just increases intense in the initial and final moments of lateral disturbance, and the overall performance is better than that of FB-FF controllers.

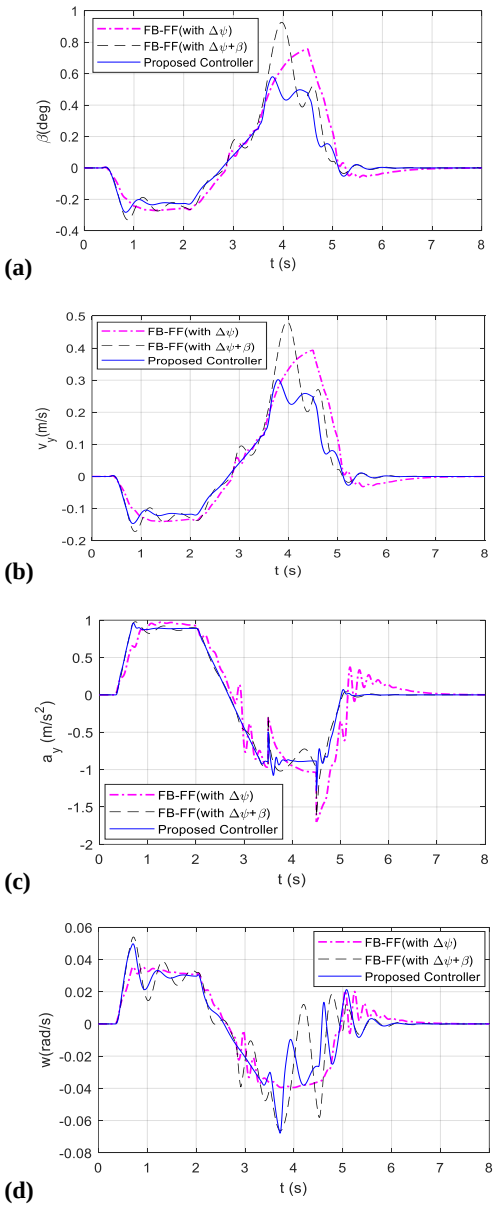

Fig. 8. The simulation results for the sideslip angle, lateral velocity, acceleration and yaw rate in the single-lane change maneuver. **(a)** Sideslip angle; **(b)** Lateral velocity; **(c)** Lateral acceleration; **(d)** Yaw rate

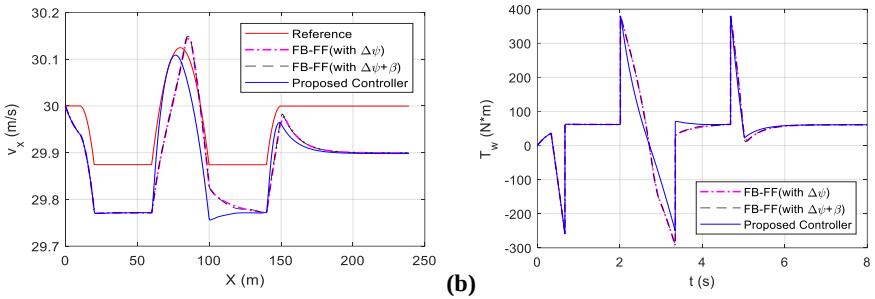

Fig. 9. The simulation results for the longitudinal velocity and control inputs in single-lane change maneuver. **(a)** Longitudinal velocity; **(b)** Total tire torques

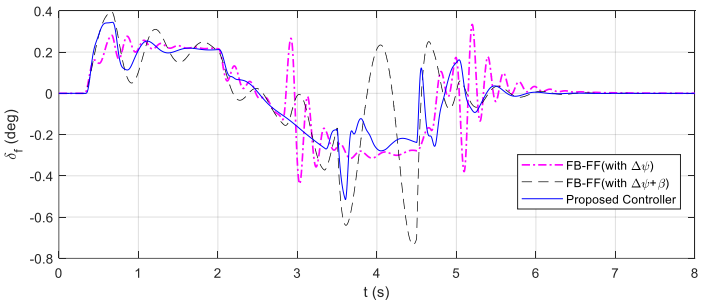

Fig. 10. The simulation results for the front-wheel steering angel in single-lane change maneuver

In addition, the single-lane change maneuver (Wang et al., 2016) on bigger curve road of different controllers is also compared. The road curvature is plotted in Figure 11(a), which is three times larger than that mentioned above. The vehicle is required to run on the high-adherence road (μ = 0.8) with initial speed of 30 m/s. The simulation results are similar with that on smaller curve road, only parts of them are shown in the paper due to length limitations. One can see from Figure 11 that the autonomous vehicle with three controllers can track the reference path and velocity approximately, but the vehicle equipped with the proposed controller performs best.

5.2. Double-Lane Change Maneuver

In this simulation case, the double-lane change maneuverer is performed on a high-adherence road μ = 0.8, with the initial speed of 22m/s. The lateral disturbance is the same as Figure 5 shows. The road curvature varying with the vehicle travel distance is presented in Figure 12(a). Figure 12(b) shows the reference longitudinal acceleration, which grows to maximum at the biggest curve similarly.

The tracking errors, vehicle states response, and control inputs with different controllers are shown in Figure 13. Similarly, as shown in sub-figure (a)-(d), the FB-FF controller with $\Delta\varphi$ performs best in the vehicle heading error response, nevertheless, yields large lateral offset and velocity heading deviation. The maximum lateral deviation is nearly 0.4m and the maximum velocity heading deviation is about 2deg, however, that of the FB-FF controller with $\Delta\varphi+\beta$ and the proposed controller can be maintained in a very small region. In contrast, the proposed controller performs best in path tracking.

Figure 14 shows the sideslip angel, lateral velocity, acceleration and yaw rate of the vehicle. It can be seen that all of the three controllers are able to keep the autonomous vehicle in stability regions after the lateral disturbance is introduced into the system. One can see that the proposed controller has the better performance than the FB-FF controller with $\Delta\varphi+\beta$ in the level of vehicle states, which guarantees more lateral stability of the vehicle. The FB-FF controller with $\Delta\varphi$ can yield smaller response of vehicle dynamics, however the increase of tracking errors is

much larger compared with the decrease of state deviations.

As shown in Figure 15 which plots the longitudinal velocity and the total tire torque that, no matter what kind of control mode is implemented, the tire torques change with the reference lateral acceleration roughly, and the tracking errors of longitudinal velocity keep the same basically. The front-wheel steering angle is plotted in Figure 16, the analysis of the front-wheel steering angle is consistent with that of the vehicle states. On the whole, the proposed controller performs best in tradeoff of trajectory tracking and lateral stability.

Moreover, the double-lane change maneuver with more sharp corners shown in (Wang et al., 2016) is completed for the vehicle. The road adhesion coefficient is set as $\mu = 0.6$ and the initial longitudinal velocity is 25m/s. Similarly, it can be seen from the Figure 17 that three controllers can yield reasonable path tracking and velocity tracking errors, among which the proposed controller performs best in trajectory tracking.

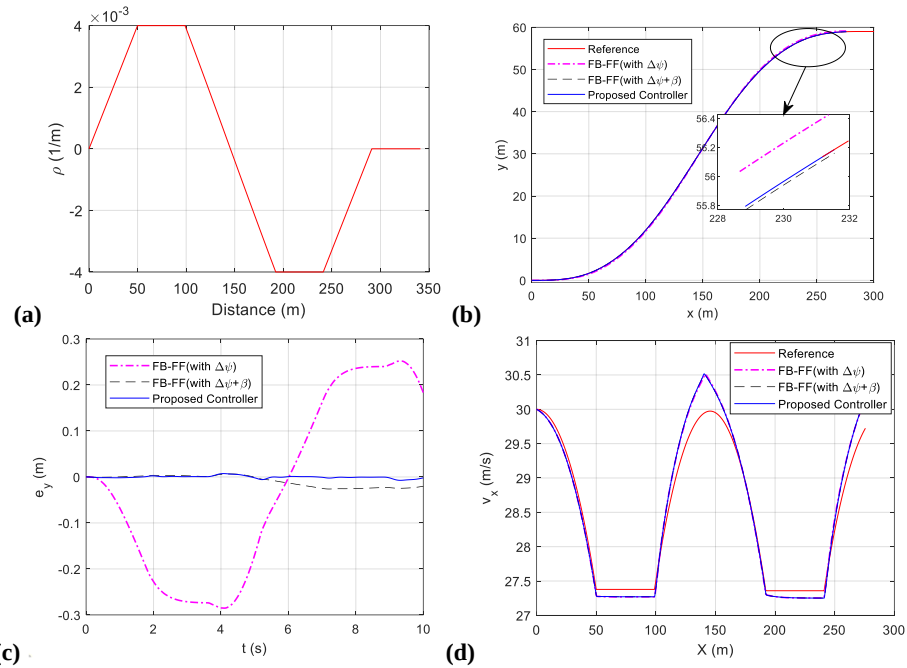

Fig. 11. The simulation results in the single-lane change maneuver on bigger curve road. **(a)** Road curvature; **(b)** Global displacement; **(c)** Lateral offset; **(d)** Longitudinal velocity

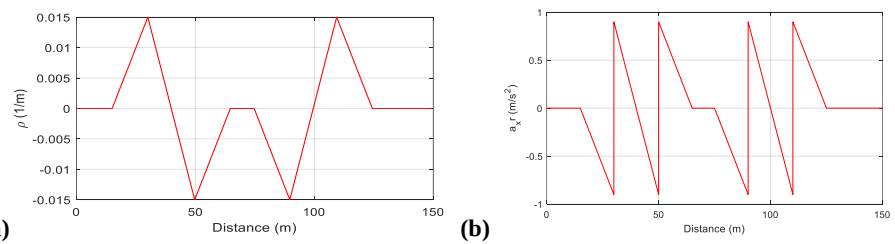

Fig. 12. Reference road curvature and longitudinal accelerations in double-lane maneuver. (a) Reference road curvature; (b) Reference longitudinal acceleration

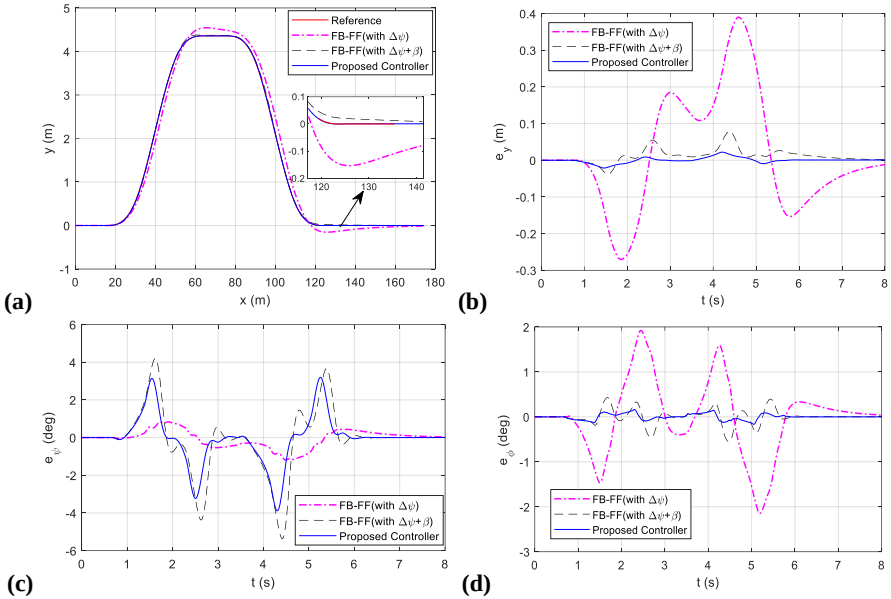

Fig. 13. The path following trajectory and tracking errors results in double-lane maneuver. (a) Path following trajectory results; **(b)** Lateral offset; **(c)** Vehicle heading error; **(d)** Velocity heading error

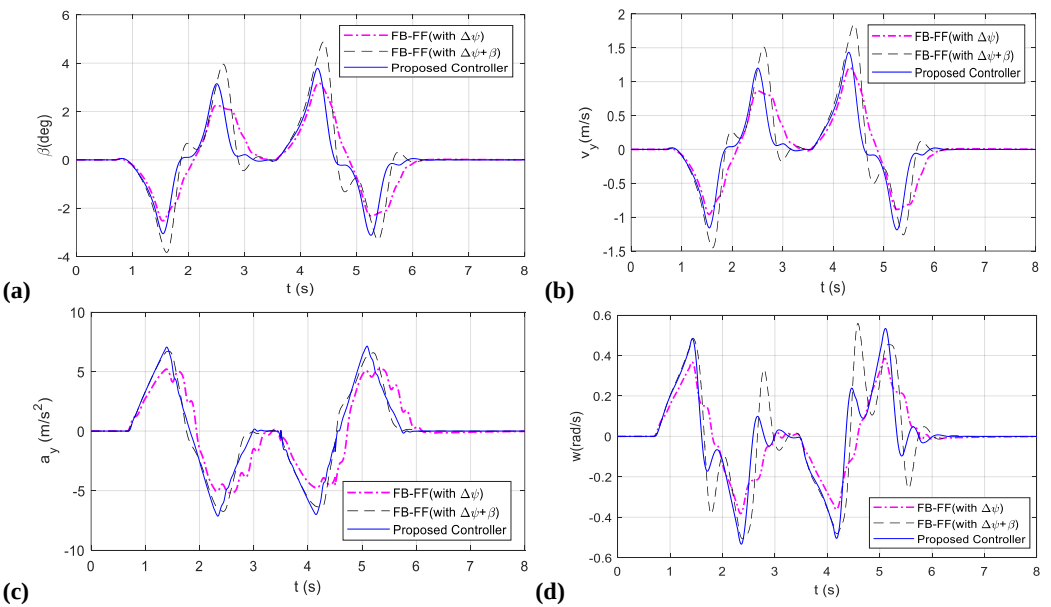

Fig. 14. The simulation results for the sideslip angle, lateral velocity, acceleration and yaw rate in the double-lane change maneuver. **(a)** Sideslip angle; **(b)** Lateral velocity; **(c)** Lateral acceleration; **(d)** Yaw rate

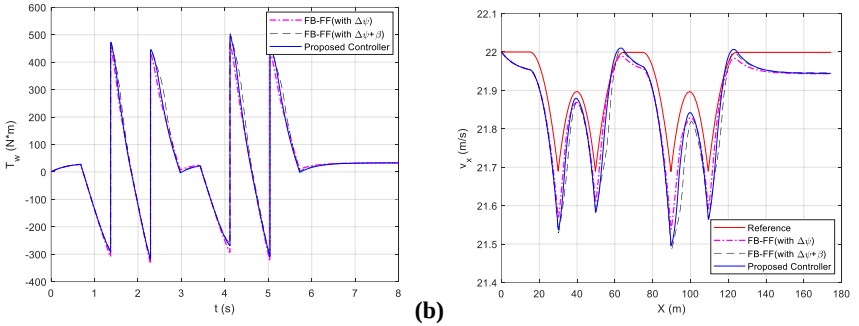

Fig. 15. The simulation results for the longitudinal velocity and control inputs in double-lane change maneuver. **(a)** Longitudinal velocity; **(b)** Total tire torques

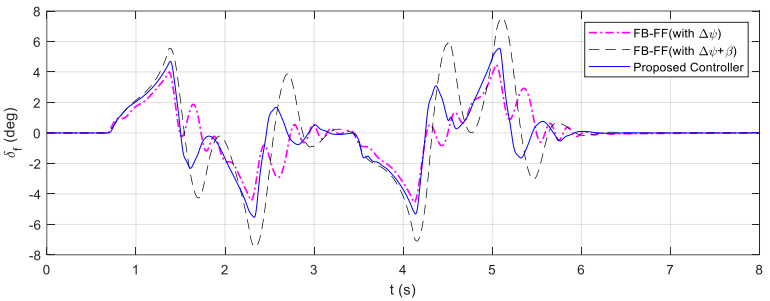

Fig. 16. The simulation results for the front-wheel steering angel in double-lane change maneuver

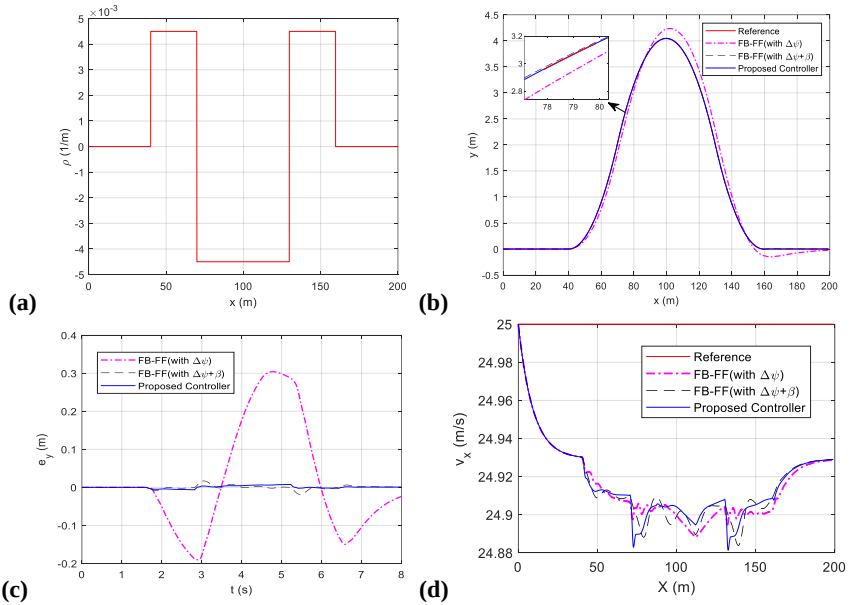

Fig. 17. The simulation results in the double-lane change maneuver with more sharp corners. **(a)** Road curvature; **(b)** Global displacement; **(c)** Lateral offset; **(d)** Longitudinal velocity

6. Conclusion

This paper proposed a robust trajectory tracking control algorithm for autonomous vehicle subject to velocity-varying and uncertain disturbance. The trajectory tracking includes two aspects: lateral path tracking and longitudinal velocity tracking before which a new reference longitudinal velocity planning method is proposed. The ADRC lateral path tracking controller and the feedforward-feedback longitudinal velocity tracking controller were designed and verified through MATLAB/Simulink. The proposed controller in this paper can accurately observe and compensate the lateral disturbance robustly and performs best in tradeoff of trajectory tracking and lateral stability.

It should be noted that our proposed control algorithm is simple and robust, thus provide great potential for engineering application. In the future, we will further carry out hardware in the loop test and real vehicle test for the proposed control algorithm.

Acknowledgments

Acknowledgments

This research was funded by the Major Scientific and Technological Innovation Project of Shandong Province (2019JZZY010911), and the National Natural Science Foundation of China Youth Fund (51905320).

Thanks to Professor Shi Shuming (https://orcid.org/0000-0001-7018-0682) and graduated postgraduate Xiang Hui in Vehicle Operation Simulation Group, Jilin University for their support of vehicle system simulation platform based on MATLAB/Simulink).

References

[1] AMER, N.H. , HAIRI, Z., 2017. *Modelling and Control Strategies in Path Tracking Control for Autonomous Ground Vehicles: A Review of State of the Art and Challenges*. Journal of Intelligent Robotic Systems, 86(2), 225-254. DOI: https://doi.org/10.1007/s10846-016-0442-0.

[2] ARDASHIR, M.D. HAMID, T., 2020. *A novel adaptive control approach for path tracking control of autonomous vehicles subject to uncertain dynamics.* Proc IMechE Part D: J Automobile Engineering, 234(8), 2115-2126. DOI: https://doi.org/10.1177/0954407019901083.

[3] BETKIER, I., MITKOW, S., KIJEK, M., 2019. *Analysis of vehicle stability loss due to strong crosswind gusts using web services in the route planning process*. Archives of Transport, 52(4), 47-56. DOI: https://doi.org/10.5604/01.3001.0014.0207.

[4] CAI, Y., ZANG, Y., SUN, X., 2018. *A Research on Lateral Extendable Preview Switching Control System for Autonomous Vehicles[J]*. Automotive Engineering, 040(009), 1032-1039. DOI: https://doi.org/10.19562/j.chinasae.qcgc.2018.09.005.

[5] CHEN, T., CHEN, L., XU, X., et al., 2019. *Simultaneous path following and lateral stability control of 4WD-4WS autonomous electric vehicles with actuator saturation*. Advances in Engineering Software, 46-54. DOI: https://doi.org/10.1016/j.advengsoft.2018.07.004.

[6] CHENG, S., LI, L., CHEN, X., et al., 2020, *Model-Predictive-Control-Based Path Tracking Controller of Autonomous Vehicle Considering Parametric Uncertainties and Velocity-Varying*. IEEE Transactions on Industrial Electronics, Early Access. DOI: https://doi.org/10.1109/TIE.2020.3009585.

[7] CHENG, S., LI, L., LIU, C.Z., et al. (2020). *Robust LMI-Based H-Infinite Controller Integrating AFS and DYC of Autonomous Vehicles With Parametric Uncertainties*. IEEE Transactions on Systems, Man, and Cybernetics, Systems, 99, 1-10. DOI: https://doi.org/10.1109/TSMC.2020.2964282.

[8] GAO, Y., GORDON, T., LIDBERG, M., 2019. *Optimal control of brakes and steering for autonomous collision avoidance using modified Hamiltonian algorithm*. Vehicle System Dynamics, 1-17. DOI: https://doi.org/10.1080/004231 14. 2018.1563706.

[9] GAO, Z. 2013. *On the foundation of active disturbance rejection control*. Control theory applications, 30.12. DOI: https://doi.org/10.7641/CTA.2013.31087.

[10] GOH, J Y., GOEL, T., GERDES, J C., 2019. *Towards Automated Vehicle Control Beyond the Stability Limits: Drifting Along a General PATH*. Journal of Dynamic Systems Measurement and Control. DOI: https://doi.org/10.1115/1.4045320.

[11] GOH, J.Y., GERDES, J.C., 2016. *Simultaneous stabilization and tracking of basic automobile drifting trajectories.* In Proceedings of the 2018 IEEE Intelligent Vehicles Symposium (IV).

[12] GUO, J., LUO, Y., LI, K., 2018. *Robust gain-scheduling automatic steering control of unmanned ground vehicles under velocity-varying motion*. Vehicle System Dynamics, 1-22. https://doi.org/10.1080/00423114.2018.1475677.

[13] GUO, L., GE, P., YUE, M., et al., 2020, *Trajectory tracking algorithm in a hierarchical strategy for electric vehicle driven by four independent in-wheel motors.* Journal of the Chinese Institute of Engineers, Early Access. DOI: https://doi.org/10.1080/02533839.2020.1819432.

[14] HAN, J.Q., 2002. *From PID technology to auto disturbance rejection control technology*. Control Engineering of China, 9(3), 13-18.

[15] HU, C., WANG, R., YAN, F., et al., 2016. *Output constraint control on path following of four-wheel independently actuated autonomous ground vehicles*. IEEE T Veh Technol, 2016,65, 4033–4043. DOI: https://doi.org/10.1109/TVT.2015.2472975.

[16] JALALI, M., KHAJEPOUR, A., CHEN, S.K., et al. 2017. *Handling Delays in Yaw Rate Control of Electric Vehicles using MPC with Experimental Verification*. Journal of Dynamic Systems Measurement Control. DOI: https://doi.org/10.1115/1.4037166.

[17] JI, X., HE, X., LV, C., et al., 2018. *Adaptive-neural-network-based robust lateral motion control for autonomous vehicle at driving limits*. Control Engineering Practice, 76(JUL.), 41-53. DOI: https://doi.org/10.1016/j.conengprac.2018.04.007.

[18] KAPANIA, N.R., GERDES, J.C., 2015. *Design of a feedback-feedforward steering controller for accurate path tracking and stability at the limits of handling*. Vehicle System Dynamics, 1-18. DOI: https://doi.org/10.1080/00423114.2015.1055279.

[19] KAPANIA, N.R., SUBOSITS, J., CHRISTIAN, G.J., 2016. *A Sequential Two-Step Algorithm for Fast Generation of Vehicle Racing Trajectories*. Journal of Dynamic Systems, Measurement, and Control, 138(9), 091005. DOI: https://doi.org/10.1115/1.4033311.

[20] LIN, F., ZHANG, Y., ZHAO, Y., et al. 2019. *Trajectory Tracking of Autonomous Vehicle with the Fusion of DYC and Longitudinal–Lateral Control*. Chinese Journal of Mechanical Engineering. DOI: https://doi.org/10.1186/s10033-019-0327-9.

[21] PACEJKA, H.B., (2006). *Tyre and Vehicle Dynamics* (5rd ed).

[22] SHIRAZI, M.M., RAD, A.B., 2018. *L1 Adaptive Control of Vehicle Lateral Dynamics[J]*. IEEE Transactions on Intelligent Vehicles, 3(1), 92-101. DOI: https://doi.org/10.1109/TIV.2017.2788186.

[23] SUN, C.; ZHANG, X.; XI, L.; TIAN, Y. 2018, Design of a Path-Tracking Steering Controller for Autonomous Vehicles. Energies, 11, 1451. https://doi.org/10.3390/en11061451.

[24] VAN, N.D., SUALEH, M., KIM, D., et al., 2020. *A Hierarchical Control System for Autonomous Driving towards Urban Challenges*. Applied Sciences, 10(10), 26. DOI: https://doi.org/ 10.3390/app10103543.

[25] WACHTER, E., ALIREZAEI, M., BRUZELIUS, F., et al., 2019. *Path control in limit handling and drifting conditions using State Dependent Riccati Equation technique*. Proceedings of the Institution of Mechanical

Engineers Part D Journal of Automobile Engineering, 095440701985073. DOI: https://doi.org/10.1177/0954407019850737.

[26] WANG, P., GAO, S., LI, L., CHENG, S., ZHAO,H., 2020. *Research on driving behavior decision making system of autonomous driving vehicle based on benefit evaluation model*. Archives of Transport, 53(1), 21-36. DOI: https://doi.org/10.5604/01.3001.0014.1740.

[27] WANG, R., HU, C., YAN, F., et al. 2016. *Composite nonlinear feedback control for path following of four-wheel independently actuated autonomous ground vehicles*. IEEE transactions on intelligent transportation systems, 17, 2063–2074. DOI: https://doi.org/10.1109/TITS.2015.2498172.

[28] WANG, R., JING, H., HU, C., et al. 2016. *Robust H∞ Path Following Control for Autonomous Ground Vehicles With Delay and Data Dropout*. IEEE Transactions on Intelligent Transportation Systems, 17(7), 2042-2050. https://doi.org/10.1109/TITS.2015.2498157.

[29] WANG, Y., SHI, S., GAO, S., et al., 2019. *Active Steering and Driving/Braking Coupled Control Based on Flatness Theory and A Novel Reference Calculation Method*. IEEE Access, 7, 180661-180670. DOI: https://doi.org/10.1109/ACCESS.2019.2959941.

[30] WU, J., CHENG, S., LIU, B., et al., 2017. *A Human-Machine-Cooperative-Driving Controller Based on AFS and DYC for Vehicle Dynamic Stability*. Energies, 10(11), 1737. DOI: https://doi.org/10.3390/en10111737.

[31] WU, Y., WANG, L., ZHANG, J., et al. 2018. *Robust vehicle yaw stability control by active front steering with active disturbance rejection controller*. Proceedings of the Institution of Mechanical Engineers Part I Journal of Systems Control Engineering. DOI: https://doi.org/10.1177/0959651818813515.

[32] WU, Y., WANG, L., ZHANG, J., et al., 2019. *Path Following Control of Autonomous Ground Vehicle Based on Nonsingular Terminal Sliding Mode and Active Disturbance Rejection Control*. IEEE Transactions on Vehicular Technology, PP(99), 1-1. DOI: https://doi.org/10.1109/TVT.2019.2916982.

[33] XIA, Y., PU, F., LI, S., et al., 2016. *Lateral Path Tracking Control of Autonomous Land Vehicle Based on ADRC and Differential Flatness*. IEEE Transactions on Industrial Electronics, 63(5), 1-1. DOI: https://doi.org/10.1109/TIE.2016.2531021.

[34] XU, Y., WANG, R., LI, B., 2001. *A summary of worldwide intelligent vehicle*. Automotive engineering, 23(5), 289-295. DOI: https://doi.org/10.19562/j.chinasae.qcgc.2001. 05.001.

[35] YAN, W., LI-FANG, W., FANG, L.I., 2019. *Intelligent vehicle path following control based on sliding mode active disturbance rejection control*. Control and Decision, DOI: https://doi.org/10.13195/j.kzyjc.2018.0179.

[36] YU Z.S., 2007. *Automobile Theory* (5rd ed). China, Beijing (Chapter 6).

[37] ZHANG, C., CHU, D., LIU, S., et al., 2019. *Trajectory Planning and Tracking for Autonomous Vehicle Based on State Lattice and Model Predictive Control*. Intelligent Transportation Systems Magazine, 11(2), 29-40. DOI: https://doi.org/10.1109/MITS.2019.2903536.

[38] ZHAO, X., CHEN, H., 2011. A study on lateral control method for the path tracking of intelligent vehicles. Qiche Gongcheng/automotive Engineering, 33(5), 382-387. DOI: https://doi.org/10.19562/j.chinasae.qcgc.2011.05.004.

[39] ZHAO, X., CHEN, H., 2011. *A study on lateral control method for the path tracking of intelligent vehicles.* Qiche Gongcheng/automotive Engineering, 33(5), 382-387. DOI: https://doi.org/10.4028/www.scientific.net/AMR. 211-212.106.